# Estimation of the Velocity of Multiple Moving Persons in Non-Stationary Indoor Environments from Received RF Signals

Rym Hicheri
*Faculty of Engineering and Science*
*University of Agder*
NO-4898 Grimstad, Norway
rym.hicheri@uia.no

Matthias Pätzold
*Faculty of Engineering and Science*
*University of Agder*
NO-4898 Grimstad, Norway
matthias.paetzold@uia.no

***Abstract*—This paper presents a new accurate iterative procedure to estimate the time-variant (TV) velocity, i.e., TV speed, TV vertical angle-of-motion (VAOM), and TV horizontal angle-of-motion (HAOM), of multiple moving objects/persons in three-dimensional (3D) non-stationary indoor propagation environments. The indoor space is assumed to be equipped with a distributed $3 \times 3$ multiple-input multiple-output (MIMO) system. The proposed procedure focuses on estimating the TV speed, TV VAOM, and TV HAOM by matching the spectrogram of the complex channel gain of a non-stationary indoor channel model to the spectrogram obtained from received radio frequency (RF) signals. Together with the velocity parameters, this method estimates all channel parameters, such as path gains, phases, etc. Numerical examples are presented to validate the proposed estimation algorithm by comparing the estimated parameters of interest with their corresponding exact quantities.**

***Index Terms*—Velocity estimation, Doppler characteristics, indoor areas, distributed MIMO systems, non-stationary channels.**

## I. Introduction

The precise estimation of the speed of mobile stations (MSs') has been shown to be a key feature in the design of several applications in mobile radio communications, such as hand-off, adaptive modulation, and power control algorithms [1]. A review of the literature [1]–[5] shows that this topic has been exhaustively investigated. The current speed estimation methods utilize different properties of the fading channels, e.g., level-crossings, covariance, correlation properties, and power spectrum, and require a priori knowledge of the statistics of the channel. Due to the small number of of statistical analyses of non-isotropic non-stationary channels, this constraint limits their applicability to wide-sense stationary channel models for which the speed is assumed to be constant. In addition, these techniques estimate only the speed of the MSs without providing any information regarding their direction of motion.

Velocity estimation has also been of central importance in the context of human in-home activity tracking and monitoring. It has been featured in numerous wireless indoor services [6]–[8], such as healthcare services, remote medical care, and home security and surveillance. There are mainly three classes of indoor activity tracking systems: video-, sensor-, and radio frequency (RF)-based devices. Video-based systems evaluate the motion of objects or persons by applying image processing techniques [9], [10]. On the other hand, sensor-based human activity tracking employs context-aware or wearable hardware sensors, e.g., accelerometers and gyroscopes [11]. One of the main drawbacks of on-body sensors is that they have to be connected to the human body. The RF-based motion tracking technique is a contactless solution which has been introduced to compensate the limitations of both video- and sensing-based methods [12]. It analyzes and leverages the effects of moving objects or persons on the Doppler characteristics of the received radio signals. The pertinence of this approach is best exemplified by the mmVital [13], the WiGait [14], and the WiFall [15] products. A brief review of radar-based indoor motion tracking approaches can be found in [16].

There has been growing attention paid to channel-state-information (CSI)-based human detection, e.g., [17]–[19]. Since most of the aforementioned studies consider pre-existing Wi-Fi infrastructures, they face several challenges [13], [16], [18], [20]. For example, the RF signal is reflected from multiple moving objects/persons in the room. This makes it difficult to distinguish between the individual contribution of each moving object/person. Hence, numerous Wi-Fi-based studies assume a single moving person in the indoor space. This assumption is not always realistic as there is usually more than one person present in indoor environments. The signal can also be reflected from fixed objects (e.g., walls, furniture, decorations), resulting in a rich scattering structure in indoor environments and need for signal processing techniques to remove the contributions of the fixed objects. The performance of RF-based systems is also sensitive to the changes in the direction of motion of the moving users. Therefore, it is of great interest to overcome these limitations. Considering the effects of both fixed and moving objects and using millimeter waves technology, a velocity estimation method has been recently proposed in [21], which is based on the two-dimensional non-stationary channel model introduced in [22]. Later, a new iterative procedure to estimate the TV velocity of a single moving person in three-dimensional (3D) indoor environments has been reported in [23], which considers the motion of a person in the vertical plane.

In this paper, we extend the algorithm developed in [23] to consider multiple moving objects/persons in an indoor environment and estimate their individual TV velocity, i.e., TV

speed, TV vertical angle-of-motion (VAOM), and TV horizontal angle-of-motion (HAOM). The propagation phenomenon taking place in the indoor space is modelled by means of the fixed-to-fixed 3D channel model in [24], which considers both fixed and moving objects. We also take into account the line-of-sight (LOS) component. Here, each moving entity (object/person) is represented by a single moving point scatterer. In the case of walking persons, the point scatterer may represent any part of the person's body, such as the center of gravity, the head, hip, or shoulder. The fixed items in the room are modelled by fixed scatterers. In the present work, we require that the indoor environment is equipped with a distributed 3×3 multiple-input multiple-output (MIMO) system, i.e., three distributed transmit antennas and three distributed receive antennas.

Here, the TV velocities, i.e, speeds and directions of motion, of the moving persons are estimated by matching the spectrograms of the considered non-stationary $3 \times 3$ MIMO channel model with the spectrograms of the received RF signals. Together with the TV velocities, the proposed iterative estimation method determines all channel parameters, including the path gains and phases as well as the TV azimuth (elevation) angles-of-departure (AAODs (EAODs)) and TV azimuth (elevation) angles-of-arrival (AAOAs (EAOAs)). These quantities are obtained by minimizing the Euclidean norm of the fitting error, which measures the difference between the spectrograms of the measured and modelled sub-channels. Besides the usefulness of the proposed algorithm in indoor human activity tracking, the determination of all channel parameters would allow the design of robust indoor channel simulators, which emulate the behavior of realistic indoor propagation scenarios in the presence of moving persons. Moreover, exact closed-form solutions have been derived for the estimates of the path gains of the moving scatterers (objects/persons) and the fixed scatterers (room items). For the performance analysis of the proposed procedure, we compare the estimated TV speed, TV VAOM, and TV HAOM with the corresponding "true" quantities. To do so, one needs the prior knowledge of the 'true" TV velocities (TV speed and TV direction of motion) of the walking persons. Exact values of these parameters are not easily available for measurement data (e.g., using wearable sensors). Hence, we will use test signals, generated by computer simulations for which the parameters of interest are known, to validate the accuracy of the estimation technique.

This paper is organized as follows. Section II presents a brief review of the non-stationary indoor channel model. The proposed iterative estimation technique is the topic of Section III. Numerical results and their discussions are presented in Section IV. Finally, Section V concludes the paper.

## II. Background Material

### A. Scenario Description

In this paper, we take advantage of the effects of a person's motion on the Doppler characteristics of propagation media and propose a new accurate procedure to estimate the TV velocity, i.e., TV speed, TV VAOM, and TV HAOM, of moving persons in a 3D indoor environment. In contrast to the algorithm developed in [23], the current estimation procedure considers the presence of multiple moving persons in the room. An example of a room architecture with six distributed antennas and two moving persons (★) is depicted in Fig. 1. Here, we denote by $A$, $B$, and $H$ the length, width, and height of the room, which is centered at the origin $O$. The indoor environment is equipped with a distributed 3×3 MIMO system, i.e., three transmit antennas ($A_1^T$, $A_2^T$, and $A_3^T$) and three receive antennas ($A_1^R$, $A_2^R$, and $A_3^R$). We employ the 3D indoor channel model reported in [24] to describe and model the propagation phenomenon taking place. For clarity, a simplified geometrical description of the propagation scenario is illustrated in Fig. 2. The fixed omni-directional antennas $A_j^T$ and $A_i^R$ are located at the positions $(x_j^T, y_j^T, z_j^T)$ and $(x_i^R, y_i^R, z_i^R)$, $i, j = 1, 2, 3$, respectively. Moreover, it is assumed that $N$ $(N \geq 1)$ objects or persons are moving in the room. Each object/person is modelled by a single moving point scatterer. The $n$th moving object/person corresponds to the $n$th moving scatterer $S_n^M$ (★), $n = 1, \ldots, N$. These moving scatterers are located at the initial positions $(x_n^M, y_n^M, z_n^M)$ and are moving with a TV velocity $\vec{v}_n(t)$. The trajectory of the $n$th moving point scatterer $S_n^M$ is determined by its TV speed $v_n(t) = |\vec{v}_n(t)|$, TV VAOM $\beta_{v,n}(t)$, and TV HAOM $\alpha_{v,n}(t)$. The TV positions $x_n(t)$, $y_n(t)$, and $z_n(t)$ along the $x$-, $y$- and $z$-axis of $S_n^M$ can be obtained according to [24, Eqs. (5)−(7)]. The scenario takes also into account the fixed objects in the room, which are modelled by $M_{ij}$ fixed scatterers $S_{m_{ij}}^F$ (•) $(m_{ij} = 1, 2, ..., M_{ij})$. The quantity $M_{ij}$ refers to the number of fixed scatterers that can be seen between the $j$th transmit antenna $A_j^T$ and the $i$th receive antenna $A_i^R$. Single-bounce scattering is assumed when modelling the moving scatterers. As is shown in Fig. 2, the TV AAOD, EAOD, AAOA, and EAOA are denoted by $\beta_{jn}^T(t)$, $\alpha_{jn}^T(t)$, $\beta_{in}^R(t)$, and $\alpha_{in}^R(t)$, respectively.

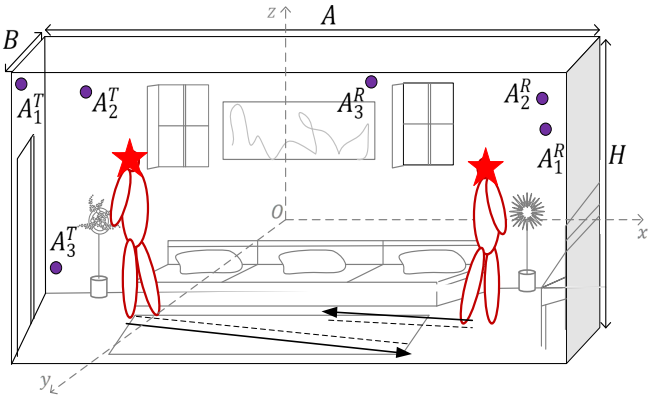


Fig. 1. Example of a typical room architecture with distributed antennas, fixed objects, and two walking persons.

### B. Non-Stationary Indoor Channel Model

In this section, we will review the analytical model employed for the simulation of realistic 3D non-stationary indoor channels. We will present the expressions for the complex channel gains $\mu_{ij}(t_p)$, Doppler frequency instances $f_{n_{ij}}(t_p)$,

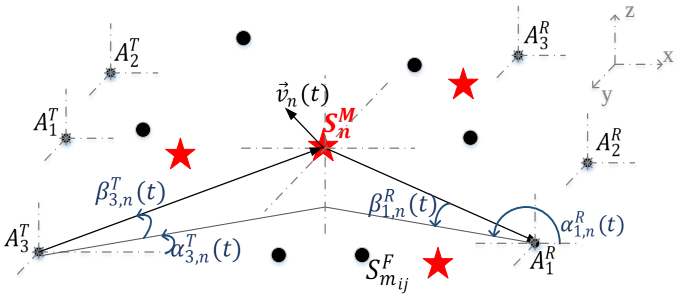


Fig. 2. Geometrical model for a non-stationary 3×3 MIMO indoor channel.

and spectrograms $S(f_q, t_p)$ sampled at discrete time instants $t_p = p\Delta t \in [0, T]$ and discrete frequencies $f_q = -B/2 + q\Delta f \in [-B/2, B/2]$, where $\Delta t$ ($\Delta f$) is the time (frequency) sampling period and $T$ ($B$) is the total observation time (bandwidth), respectively. Assuming perfect CSI at the receivers side, the discrete complex channel gain $\mu_{ij,p} = \mu_{ij}(t_p)$ between the $j$th transmit antenna and $i$th receive antenna $(i, j = 1, 2, 3)$ can be expressed [24, Eq. (27)] as

$$\mu_{ij}(t_p) = \sum_{n=1}^{N} c_{ijn} \exp[j\theta_{ijn}(t_p)] + \sum_{m=0}^{M_{ij}} a_{ijm} \exp(j\vartheta_{ijm}) . \quad (1)$$

Here, the first term describes the components associated with the $N$ moving scatterers $S_n^M$ $(n = 1, \ldots, N)$, and the second term refers to the sum of the multipath propagation components resulting from the $M_{ij}$ fixed scatterers $S_{ijm}^F$ $(m_{ij} = 0, \ldots, M_{ij})$. Since the positions of both the transmit antennas $A_j^T$ and receive antennas $A_i^R$ are fixed, the LOS component does not experience any Doppler shift. Hence, can be modelled as a fixed component with gain $a_{ij0}$ and phase $\vartheta_{ij0}$ and is included in the second term of (1). The quantity $c_{ijn}$ ($a_{ijm}$) denotes the fixed path gain of the $n$th ($m$th) moving scatterer (fixed scatterer between $A_j^T$ and $A_i^R$). The phases $\vartheta_{ijm}$ are assumed to be independent and identically distributed random variables which follow the uniform distribution over the interval $(0, 2\pi]$. In (1), the TV phases $\theta_{ijn}(t_p) = \theta_{ijn,p} = 2\pi \int_0^{t_p} f_{ijn}(u)du + \theta_{ijn,0}$ are stochastic processes, where $f_{ijn}(t_p) = f_{ijn,p}$ is the TV Doppler frequency caused by the motion of the $n$th moving scatterer $S_n^M$, and $\theta_{ijn,0}$ is the initial phase of the $n$th multipath component at the time instant $t_p = 0$. According to [24, Eq. (18)], the TV Doppler frequencies $f_{ijn,p}$ are given by $f_{ijn,p} = -f_0 v_{n,p}\{\cos(\beta_{v,n,p})[\cos(\beta_{jn,p}^T)\cos(\alpha_{jn,p}^T - \alpha_{v,n,p})\cos(\alpha_{jn,p}^T - \alpha_{v,n,p}) + \cos(\beta_{in,p}^R)\cos(\alpha_{in,p}^R - \alpha_{v,n,p})] + \sin(\beta_{v,n,p})[\sin(\beta_{in,p}^R) + \sin(\beta_{jn,p}^T)]\}/c_0$. Here, $v_{n,p} = v_n(t_p)$ is the TV speed of $S_n^M$ at the time instant $t_p$ and the quantities $f_0$ and $c_0$ denote the carrier frequency and the speed of light, respectively. The TV angles $\beta_{jn,p}^T = \beta_{jn}^T(t_p)$, $\alpha_{jn,p}^T = \alpha_{jn}^T(t_p)$, $\beta_{in,p}^R = \beta_{in}^R(t_p)$, and $\alpha_{in,p}^R = \alpha_{in}^R(t_p)$ can be expressed in terms of the TV positions of the moving scatterers and the positions of the distributed transmit and receive antennas as detailed in [24, Eqs. (10)−(13)].

### C. Spectrogram

The main goal of this work is to estimate the TV velocity $\vec{v}_n(t_p)$ of the moving persons, represented by $S_n^M$, $n = 1, \ldots, N$, from the complex channel gains $\mu_{ij}(t_p)$while taking into account the overall effect of the fixed scatterers, regardless of the individual contribution of each fixed scatterer $S_{ijm}^F$, $m = 1, .., M_{ij}$. In the following, the overall effect of the fixed scatterers (second part of (1)) will be described using the single complex term $C_{F_{ij}} \exp(j\vartheta_{F_{ij}})$, where $C_{F_{ij}} = ((\sum_{m=0}^{M_{ij}} a_{ijm}\cos(\vartheta_{ijm}))^2 + (\sum_{m=0}^{M_{ij}} a_{ijm}\sin(\vartheta_{ijm}))^2)^{1/2}$ and $\vartheta_{F_{ij}} = \text{atan2}(\sum_{m=0}^{M_{ij}} a_{ijm}\sin(\vartheta_{ijm}), \sum_{m=0}^{M_{ij}} a_{ijm}\cos(\vartheta_{ijm}))$, in which atan2 stands for the inverse tangent function that returns the angle in the interval $[-\pi, pi)$. According to [24], by approximating the Doppler frequencies $f_{ijp}$ by $K$ piecewise linear functions, the spectrogram $S_{ij}(f_q, t_p)$ of $\mu_{ij}(t_p)$ can be expressed as

$$S_{ij}(f_q, t_p) = S_{ij}^{(a)}(f_q, t_p) + S_{ij}^{(c)}(f_q, t_p) \quad (2)$$

where $S_{ij}^{(a)}(f, t)$ and $S_{ij}^{(c)}(f, t)$ are called the auto-term and the cross-term of the spectrogram, respectively. The auto-term $S_{ij}^{(a)}(f, t)$ is given by

$$S_{ij}^{(a)}(f_q, t_p) = \sum_{n=1}^{N} c_{ijn}^2 G(f, f_{ijn,p}, \sigma_{ijn,1,p}^2) + G\left(f, 0, \frac{\sigma_0^2}{2}\right) C_{F_{ij}}^2 \quad (3)$$

where $G(a, b, c) = \exp[-(a-b)^2/(2c)]/(\sqrt{2\pi c})$, $\sigma_0^2 = 1/(2\pi\sigma_w)^2$, and $\sigma_{ijn,1,p}^2 = (\sigma_0^2 + \sigma_w^2 k_{ijn,p}^2)/2$, in which $k_{ijn,p} = k_{ijn}(t_p)$ is defined in [24, Eq. (25)] and $\sigma_w^2$ is the spread of the Gaussian window utilized for the computation of the spectrogram [24, Eq. (30)]. The cross-term $S_{ij}^{(c)}(f_q, t_p)$ is expressed as in (4) [see the top of the next page], where the operator $\Re\{\cdot\}$ denotes the real part of a complex function and $\sigma_{ijn,2,p}^2 = \sigma_0^2 - jk_{ijn,p}/(2\pi)$.

A new method to estimate the TV velocity of moving persons in indoor areas will be presented in the following section, based on the Doppler properties of the channel model described by (1).

## III. Estimation of the Time-Variant Velocity

In reality, the complex channel gain $\hat{\mu}_{ij,p} = \hat{\mu}_{ij}(t_p)$ is computed from samples of the measured received RF signal at discrete time instances $t_p$. Then, the corresponding spectrogram $\hat{S}_{ij}(f_q, t_p)$, which is sampled at discrete time instances $t_p$ and discrete frequencies $f_q$, is computed according to the procedure described in [24, Section IV]. The problem at hand here is to determine, at each time instant $t_p$, a set of parameters $\mathcal{P}_p = \{c_{ijn}, k_{ijn,p}, \theta_{ijn,0}, C_{F_{ij}}, \vartheta_{F_{ij}}, v_{n,p}, \alpha_{jn,p}^T, \beta_{jn,p}^T, \alpha_{in,p}^R, \beta_{in,p}^R, \alpha_{v,n,p}, \beta_{v,n,p}\}$, $i, j = 1, 2, 3$ and $n = 1, \ldots, N$, in such a way that the spectrogram $S_{ij}(f_q, t_p)$ of $\mu_{ij}(t_p)$ [see (3)] matches the spectrogram $\hat{S}_{ij}(f_q, t_p)$ of the measured channel. For this purpose, we introduce the objective function for determining $\mathcal{P}_p$ as

$$E(\mathcal{P}_p) = \sum_{i,j=1}^{3} \left|\left| \hat{S}_{ij}(f_q, t_p) - S_{ij}(f_q, t_p) \right|\right|_2^2 . \quad (5)$$

$$S_{ij}^{(c)}(f_q,t_p)=\frac{2}{\sigma_w\sqrt{\pi}}\left[\sum_{n=1}^{N}\sum_{k=n+1}^{N}c_{ijn}c_{ijk}\Re\left\{G\left(f_q,f_{ijn,p},\sigma_{ijn,2,p}^2\right)G^*\left(f_q,f_{ijk,p},\sigma_{ijk,2,p}^2\right)\exp\left(j\left(\theta_{ijn,p}-\theta_{ijk,p}\right)\right)\right\}\right.$$
$$\left.+C_{F_{ij}}\sum_{n=1}^{N}c_{ijn}G\left(f_q,0,\sigma_0^2\right)\Re\left\{G\left(f_q,f_{ijn,p},\sigma_{ijn,2,p}^2\right)\exp\left(j\left(\theta_{ijn,p}-\vartheta_{F_{ij}}\right)\right)\right\}\right] \quad (4)$$

$$E(\mathcal{P}_p)=\sum_{i,j=1}^{3}\left\|\hat{\mathbf{S}}_{ij}-\sum_{n=1}^{N}c_{ijn}^2G\left(f_q,f_{ijn,p},\sigma_{ijn,1,p}^2\right)-\mathbf{G}C_{F_{ij}}^2-\frac{2}{\sigma_w\sqrt{\pi}}\left[\sum_{n=1}^{N-1}\sum_{k=n+1}^{N}c_{ijn}c_{ijk}\Re\left\{G\left(f_q,f_{ijn,p},\sigma_{ijn,2,p}^2\right)\exp(j\theta_{ijn,p})\right.\right.\right.$$
$$\left.\left.\left.\cdot\exp(-j\theta_{ijk,p})\,G^*\left(f_q,f_{ijk,p},\sigma_{ijk,2,p}^2\right)\right\}+C_{F_{ij}}\sum_{n=1}^{N}c_{ijn}G\left(f_q,0,\sigma_0^2\right)\Re\left\{G\left(f_q,f_{ijn,p},\sigma_{ijn,2,p}^2\right)\exp\left(j\left(\theta_{ijn,p}-\vartheta_{F_{ij}}\right)\right)\right\}\right]\right\|_2^2 \quad (6)$$

$$h_{ijn_0}^{(l)}(f_q,t_p)=\hat{\mathbf{S}}_{ij}-\sum_{\substack{n=1\\n\neq n_0}}^{N}\left(c_{ijn}^{(l)}\right)^2G\left(f_q,f_{ijn,p}^{(l)},\left(\sigma_{ijn,1,p}^{(l)}\right)^2\right)-\frac{2}{\sigma_w\sqrt{\pi}}\left[\sum_{\substack{n=1\\n\neq n_0}}^{N-1}\sum_{k=n+1}^{N}c_{ijn}^{(l)}c_{ijk}^{(l)}\Re\left\{G\left(f_q,f_{ijn,p}^{(l)},\left(\sigma_{ijn,2,p}^{(l)}\right)^2\right)\exp\left(j\theta_{ijn,p}^{(l)}\right)\right.\right.$$
$$\left.\left.\cdot\exp\left(-j\theta_{ijk,p}^{(l)}\right)G^*\left(f_q,f_{ijk,p}^{(l)},\left(\sigma_{ijk,2,p}^{(l)}\right)^2\right)\right\}+C_{F_{ij}}^{(l)}\sum_{\substack{n=1\\n\neq n_0}}^{N}c_{ijn}G\left(f_q,0,\sigma_0^2\right)\Re\left\{G\left(f_q,f_{ijn,p}^{(l)},\left(\sigma_{ijn,2,p}^{(l)}\right)^2\right)\exp\left(j\left(\theta_{ijn,p}^{(l)}-\vartheta_{F_{ij}}^{(l)}\right)\right)\right\}\right] \quad (7)$$

$$\left(c_{ijn_0}^{(l+1)},k_{ijn_0,p}^{(l+1)},\theta_{ijn_0,0}^{(l+1)},C_{F_{ij}}^{(l+1)},\vartheta_{F_{ij}}^{(l+1)},v_{n_0,p}^{(l+1)},\beta_{v,n_0,p}^{(l+1)},\alpha_{v,n_0,p}^{(l+1)},(\beta_{jn_0,p}^T)^{(l+1)},(\alpha_{jn_0,p}^T)^{(l+1)},(\beta_{in_0,p}^R)^{(l+1)},(\alpha_{in_0,p}^R)^{(l+1)}\right)=$$
$$\underset{\mathcal{P}_p}{\operatorname{argmin}}\left\{\sum_{i,j=1}^{3}\left\|\hat{\mathbf{H}}_{ijn_0,p}^{(l)}-c_{ijn_0}^2G\left(f_q,f_{ijn_0,p},\sigma_{ijn_0,1,p}^2\right)-\mathbf{G}C_{F_{ij}}^2-\frac{2}{\sigma_w\sqrt{\pi}}\left[\sum_{k=n_0+1}^{N}c_{ijn_0}c_{ijk}\Re\left\{G\left(f_q,f_{ijn_0,p},\sigma_{ijn_0,2,p}^2\right)\right.\right.\right.\right.$$
$$\left.\left.\left.\left.\cdot\exp\left(j\left(\theta_{ijn_0,p}-\theta_{ijk,p}\right)\right)G^*\left(f_q,f_{ijk,p}^{(l)},\sigma_{ijk,2,p}^2\right)\right\}+C_{F_{ij}}c_{ijn_0}G\left(f_q,0,\sigma_0^2\right)\Re\left\{G\left(f_q,f_{ijn_0,p},\sigma_{ijn_0,2,p}\right)\exp\left(j\left(\theta_{ijn,p}^{(l)}-\vartheta_{F_{ij}}\right)\right)\right\}\right]\right\|_2^2\right\} \quad (8)$$

Inserting (3) and (4) in (5), the objective function $E(\mathcal{P}_p)$ can be alternatively written as in (6) [see the top of this page], where $\hat{\mathbf{S}}_{ij}$ and $\mathbf{G}$ are column vectors containing the stacked values of $\hat{S}_{ij}(f_q,t_p)$ and $G(f_q,0,\sigma_0^2/2)$ for increasing values of $q$, respectively. Starting with $N=n_0=1$ and choosing arbitrary initial values for $c_{ijn_0}^{(0)}$, $k_{ijn_0,p}^{(0)}$, $\theta_{ijn_0,0}^{(0)}$, $C_{F_{ij}}^{(0)}$, $\vartheta_{F_{ij}}^{(0)}$, $v_{n_0,p}^{(0)}$, $\beta_{v,n_0,p}^{(0)}$, $\alpha_{v,n_0,p}^{(0)}$, $(\beta_{jn_0,p}^T)^{(0)}$, $(\alpha_{jn_0,p}^T)^{(0)}$, $(\beta_{in_0,p}^R)^{(0)}$, and $(\alpha_{in_0,p}^R)^{(0)}$ $(i,j=1,2,3$ and $n=1,\ldots,N)$, we introduce the error functions $h_{ijn_0}^{(l)}(f_q,t_p)$ for the $n_0$th moving scatterer $S_{n_0}^M$ at every iteration $l$ $(l=1,2,\ldots)$ as in (7) [see the top of this page]. Then, the new estimates of $c_{ijn_0}^{(l+1)}$, $k_{ijn_0,p}^{(l+1)}$, $\theta_{ijn_0,0}^{(l+1)}$, $C_{F_{ij}}^{(l+1)}$, $\vartheta_{F_{ij}}^{(l+1)}$, $v_{n_0,p}^{(l+1)}$, $\beta_{v,n_0,p}^{(l+1)}$, $\alpha_{v,n_0,p}^{(l+1)}$, $(\beta_{jn_0,p}^T)^{(l+1)}$, $(\alpha_{jn_0,p}^T)^{(l+1)}$, $(\beta_{in_0,p}^R)^{(l+1)}$, and $(\alpha_{in_0,p}^R)^{(l+1)}$ are obtained according to (8) [see the top of this page]. For fixed values of $c_{ijn_0}^{(l)}$, $k_{ijn_0,p}^{(l)}$, $\theta_{ijn_0,0}^{(l)}$, $C_{F_{ij}}^{(l)}$, $\vartheta_{F_{ij}}^{(l)}$, $v_{n_0,p}^{(l)}$, $\beta_{v,n_0,p}^{(l)}$, $\alpha_{v,n_0,p}^{(l)}$, $(\beta_{jn_0,p}^T)^{(l)}$, $(\alpha_{jn_0,p}^T)^{(l)}$, $(\beta_{in_0,p}^R)^{(l)}$, and $(\alpha_{in_0,p}^R)^{(l)}$, one can derive the right-hand side of (8) with respect to the variable $c_{ijn_0}$, which shows that (8) reaches a minimum if the new estimate $c_{ijn_0}^{(l+1)}$ satisfies the following cubic equation

$$a_0\left(c_{ijn_0}^{(l+1)}\right)^3+b_0\left(c_{ijn_0}^{(l+1)}\right)^2+c_0c_{ijn_0}^{(l+1)}+d_0=0 \quad (9)$$

where $a_0=2||\mathbf{y}_{ijn_0}^{(l)}||_2^2$, $b_0=3(\mathbf{y}_{ijn_0}^{(l)})^T\mathbf{f}_{ij}^{(l)}$, $c_0=||\mathbf{f}_{ij}^{(l)}||_2^2-2(\hat{\mathbf{H}}_{ijn_0,p}^{(l)}-\mathbf{G}(C_{F_{ij}}^{(l)})^2)^T\mathbf{y}_{ijn_0}^{(l)}$, and $d_0=(\mathbf{f}_{ij}^{(l)})^T[\hat{\mathbf{H}}_{ijn_0,p}^{(l)}-\mathbf{G}(C_{F_{ij}}^{(l)})^2]$, with $(\cdot)^T$ being the transpose operator. Here, $\mathbf{f}_{ij}^{(l)}$ and $\mathbf{y}_{ijn_0}^{(l)}$ are column vectors containing the stacked values of the functions $2[\sum_{k=n_0+1}^{N}c_{ijk}\ \Re\{G(f_q,f_{ijn_0,p},\sigma_{ijn_0,2,p}^2)\exp(j(\theta_{ijn_0,p}-\theta_{ijk,p}))G^*(f_q,f_{ijk,p}^{(l)},\sigma_{ijk,2,p}^2)\}+\ \Re\{G(f_q,f_{ijn_0,p},\sigma_{ijn_0,2,p})\exp(j(\theta_{ijn_0,p}^{(l)}-\vartheta_{F_{ij}}))\}C_{F_{ij}}G(f_q,0,\sigma_0^2)]/(\sigma_w\sqrt{\pi})$ and $G(f_q,f_{ijn_0,p}^{(l)},(\sigma_{ijn_0,1,p}^{(l)})^2)$, respectively, for increasing values of $q$. Since the coefficients $a_0$, $b_0$, $c_0$, and $d_0$ of (9) are real, one can state that at least one of its roots $x_k$ $(k=1,2,3)$ is real. These roots $x_k$ can be expressed as $x_k=-(b_0+\zeta^kA_0+B_0/(\zeta^kA_0))/(3a_0)$, where $\zeta$ is a cube root of unity, $B_0=b_0^2-3a_0c_0$, and $A_0=[(C_0\pm\sqrt{-27\Delta_0a_0^2})/2]^{1/3}$, in which the quantity $C_0$ is given by $C_0=2b_0^3-9a_0b_0c_0+27a_0^2d_0$, and the discriminant $\Delta_0$ is expressed as $\Delta_0=18a_0b_0c_0d_0-4b_0^3d_0+b_0^2c_0^2-4a_0c_0-27a_0^2d_0^2$. Then, the new estimate of the gain $c_{ijn_0}^{(l+1)}$ of the moving scatterer $S^M$ corresponds to the real-valued root $x_k$ that minimizes the right-hand side of (8). Similarly, it can be shown that (8) is minimized if the new estimate $C_{F_{ij}}^{(l+1)}$ satisfies

$$a_1\left(C_{F_{ij}}^{(l+1)}\right)^3+b_1\left(C_{F_{ij}}^{(l+1)}\right)^2+c_1C_{F_{ij}}^{(l+1)}+d_1=0 \quad (10)$$

where $a_1=2\,||\mathbf{G}||^2$, $b_1=3\mathbf{G}^T\mathbf{k}_{ij}^{(l)}$, $c_1=||\mathbf{k}_{ij}^{(l)}||^2-2(\hat{\mathbf{S}}_{ij}-\mathbf{v}_{ij}^{(l)}-\mathbf{u}_{ij}^{(l)})^T\mathbf{G}$, and $d_1=-(\mathbf{k}_{ij}^{(l)})^T(\hat{\mathbf{S}}_{ij}-\mathbf{v}_{ij}^{(l)}-\mathbf{u}_{ij}^{(l)})$, in which $\mathbf{k}_{ij}^{(l)}$, $\mathbf{v}_{ij}^{(l)}$ and $\mathbf{u}_{ij}^{(l)}$ refer to the column vectors containing the stacked values of the functions $\sum_{n=1}^{N}c_{ijn}^{(l+1)}\Re\{G(f_q,f_{ijn,p},\sigma_{ijn,2,p})\,G(f_q,0,\sigma_0^2)\exp(-j(\vartheta_{F_{ij}}-\theta_{ijn,p}))\}2/(\sigma_w\sqrt{\pi})$, $\sum_{n=1}^{N}c_{ijn}^2G(f_q,f_{ijn,p},\sigma_{ijn,1,p}^2)$, and

$$\Big(k_{ijn_0,p}^{(l+1)},\theta_{ijn_0,0},\vartheta_{F_{ij}}^{(l+1)},v_{n_0,p}^{(l+1)},\beta_{v,n_0,p}^{(l+1)},\alpha_{v,n_0,p}^{(l+1)},(\beta_{jn_0,p}^{T})^{(l+1)},(\alpha_{jn_0,p}^{T})^{(l+1)},(\beta_{in_0,p}^{R})^{(l+1)},(\alpha_{in_0,p}^{R})^{(l+1)}\Big)=$$

$$\underset{\mathcal{P}_p\setminus\{c_{ijn_0},C_{F_{ij}}\}}{\operatorname{argmin}}\left\{\sum_{i,j=1}^{3}\left\|\hat{\mathbf{H}}_{ijn_0,p}^{(l)}-c_{ijn_0}^2G\big(f_q,f_{ijn_0,p},\sigma_{ijn_0,1,p}^2\big)-\mathbf{G}C_{F_{ij}}^2-\frac{2}{\sigma_w\sqrt{\pi}}\Bigg[\sum_{k=n_0+1}^{N}c_{ijn_0}c_{ijk}\Re\big\{G\big(f_q,f_{ijn_0,p},\sigma_{ijn_0,2,p}^2\big)\right.\right.$$

$$\left.\left.\cdot\exp\big(j(\theta_{ijn_0,p}-\theta_{ijk,p})\big)G^*\Big(f_q,f_{ijk,p}^{(l)},\sigma_{ijk,2,p}^2\Big)\big\}+C_{F_{ij}}c_{ijn_0}G\big(f_q,0,\sigma_0^2\big)\Re\big\{G(f_q,f_{ijn_0,p},\sigma_{ijn_0,2,p})\exp\big(j(\theta_{ijn,p}-\vartheta_{F_{ij}})\big)\big\}\Bigg]\right\|_2^2\right\} \quad (11)$$

$[2/(\sigma_w\sqrt{\pi})]\sum_{n=1}^{N-1}\sum_{k=n+1}^{N}c_{ijn}c_{ijk}\Re\{G(f_q,f_{ijn,p},\sigma_{ijn,2,p}^2)$ $\exp(j(\theta_{ijn,p}-\theta_{ijk,p}))G^*(f_q,f_{ijk,p}^{(l)},\sigma_{ijk,2,p}^2)\}$ for increasing values of $q$, respectively. The expressions of the real or/and complex roots $x_k$ $(k=1,2,3)$ of (10) are given by $x_k=-(b_1+\zeta^kA_1+B_1/(\zeta^kA_1))/(3a_1)$, where $B_1=b_1^2-3a_1c_1$, and $A_1=[(C_1\pm\sqrt{-27\Delta_1a_1^2})/2]^{1/3}$, with $C_1=2b_1^3-9a_1b_1c_1+27a_1^2d_1$, and $\Delta_1=18a_1b_1c_1d_1$ $-4b_1^3d_1+b_1^2c_1^2-4a_1c_1-27a_1^2d_1^2$. Then, the new estimate $C_{F_{ij}}^{(l+1)}$ corresponds to the non-negative real-valued root $x_k$ of (10) that is the global minimum of the right-hand side of (8). Inserting the new estimates $c_{ijn_0}^{(l+1)}$ and $C_{F_{ij}}^{(l+1)}$ in (8), we obtain the reduced optimization problem in (11) [see the top of this page]. Finally, the new estimates of the remaining parameters are numerically computed according to (11). The steps in (5)−(11) proceed as long as the relative change $|E^{(l+1)}(\mathcal{P}_p)-E^{(l)}(\mathcal{P}_p)|^2$ of the objective function $E(\mathcal{P}_p)$ is higher than the predefined error level $\varepsilon$. If the relative change $|E^{(l+1)}(\mathcal{P}_p)-E^{(l)}(\mathcal{P}_p)|^2$ in the objective function is smaller than $\varepsilon$, the number of moving scatterers $N$ is incremented by 1, i.e., $N\longleftarrow N+1$. By considering new initial values for the parameters corresponding to the $N$th moving person $c_{ijN}^{(0)}$, $k_{ijN,p}^{(0)}$, $\theta_{ijN,0}^{(0)}$, $v_{N,p}^{(0)}$, $\beta_{v,N,p}^{(0)}$, $\alpha_{v,N,p}^{(0)}$, $(\beta_{jN,p}^{T})^{(0)}$, $(\alpha_{jN,p}^{T})^{(0)}$, $(\beta_{iN,p}^{R})^{(0)}$, and $(\alpha_{iN,p}^{R})^{(0)}$, we define a new error function $h_{ijN}^{(0)}(f_q,t_p)$, whose expression can be obtained from (7) by replacing $n_0$ by $N$. Then, the new estimates of the parameters of interest can be computed following the steps (5)−(11). This iterative procedure is repeated until the increase of the number of moving scatterers $N$ does not further decrease the objective function $E(\mathcal{P}_p)$ (the relative change of the function $E(\mathcal{P}_p)$ is smaller than or equal to $\varepsilon$) or a predefined maximum number of moving scatterers $N_{\max}$ is reached.

Finally, it should be mentioned that, due to the non-stationary behavior of indoor channels, the proposed estimation method for the TV velocities needs to be performed at each time instant $t_p$.

## IV. Numerical Results

The validation of the proposed velocity estimation algorithm is the topic of this section. To do so, we present numerical results comparing the exact TV Doppler frequencies, TV speed, and TV VAOM with the corresponding estimated quantities. This task cannot be achieved with measurement data, for which the accurate channel parameters, including the TV velocity of the person, are not always known. To ensure a fair evaluation of the iterative estimation method explained in Section III, we will consider sample functions of the complex channel gains $\hat{\mu}_{ij}(t_p)$, generated by means of computer simulations. Then, we will compute the corresponding spectrograms $\hat{S}_{ij}(f_q,t_p)$ according to the framework for activity monitoring based on the Doppler characteristics of indoor channels reported in [24]. The values of the parameters used in the following figures are presented in Table I and have been chosen according to [25] and [26].

We start by describing the scenario considered for the performance analysis. This scenario consists of a room of length $A$, width $B$, and height $H$. The fixed omni-directional antennas $A_1^T$, $A_2^T$, $A_3^T$, $A_1^R$, $A_2^R$, and $A_3^R$ are located at the positions $(5,2.5,2.25)$, $(-5,2.5,2.25)$, $(5,-2.5,-2.25)$, $(5,2.5,2.25)$, $(5,2.5,-2.25)$, and $(-5,-2.5,2.25)$, respectively. Here, we consider two moving persons, $P_1$ and $P_2$, who start walking from opposite corners of the room. Each person $P_n$ is modelled by a single moving point scatterers $S_n^M$ $(n=1,2)$, which represents the person's head. According to [25], the head trajectory of the walking person $P_n$ can be modelled as $z_n(t)=h_{\text{step},n}\cos(2\pi f_{\text{step},n}t)+h_{\text{head},n}$, where $h_{\text{step},n}$ and $h_{\text{head},n}$ are the step height and the height of $P_n$, $n=1,2$. Here, $f_{\text{step}}$ is the walking frequency and is equivalent to the horizontal speed $V_{\text{H},n}$ over the step length $L_{\text{step},n}$. The observation time duration is 4 s. For simplicity, we assume the persons' trajectories in the $xy$-plane to be linear. The movement of person $P_1$ can be divided into three phases. In this first phase, the person starts walking with a constant speed for 2.5 s (corresponds approximately to a distance of 2 m). In the second phase, he/she starts falling until he/she lies on the floor. The fall phase lasts 1 s. For the rest of the observation time, the person $P_1$ lies completely on the floor and is no longer moving. The person $P_2$ walks with constant speed during the total observation time. The parameter $\sigma_w^2$ has been chosen to be $\sigma_w^2=\min(1/\sqrt{2\pi|k_{ij}(t_l)|})$. The TV HAOM $\alpha_{v,n}(t)$ and TV VAOM $\beta_{v,n}(t)$ of the person $P_n$ have been computed in terms of the initial and final locations of the moving scatterer $S_n^M$.

Figs. 3(a) and (b) illustrate the "true" or exact TV speed $v_n(t)$, $n=1,2$, of the moving persons $P_1$ and $P_2$ (modelled by the scatterers $S_1^M$ and $S_2^M$, respectively) together with the corresponding estimated values. The good fit between the exact TV speed and the estimated TV speed verifies the validity and accuracy of the proposed iterative estimation technique. Together with the TV velocity, i.e., TV speed and TV direction of motion, the acceleration (as well as

TABLE I
SIMULATION PARAMETERS

| Symbol | Name | Value |
|---|---|---|
| $A$ | Room length | 10 m |
| $B$ | Room width | 5 m |
| $H$ | Room height | 2.4 m |
| $N$ | Number of moving scatterers | 2 |
| $M_{ij}$ | Number of fixed scatterers between $A_j^T$ and $A_i^R$ | 7 |
| $c_{ijn}$ | Path gain of the $n$th moving scatterer $S_n^M$ | 1 |
| $a_{ijm}$ | Path gain of the $m_{ij}$th fixed scatterer $S_{m_{ij}}^F$ | $\sqrt{1/M_{ij}}$ |
| $h_{\text{head},1}$ | Height of person $P_1$ | 1.60 m |
| $h_{\text{head},2}$ | Height of person $P_2$ | 1.60 m |
| $h_{\text{step},2}$ | Step height of person $P_1$ (young adult) | 3.2 cm |
| $h_{\text{step},1}$ | Step height of person $P_2$ (elderly person) | 2.7 cm |
| $L_{\text{step},2}$ | Step length of person $P_1$ (young adult) | 66 cm |
| $L_{\text{step},1}$ | Step length of person $P_2$ (elderly person) | 35 cm |
| $V_{\text{H},2}$ | Horizontal speed of person $P_1$ (young adult) | 0.8 m/s |
| $V_{\text{H},1}$ | Horizontal speed of person $P_2$ (elderly person) | 0.8 m/s |
| $f_0$ | Carrier frequency | 5.9 GHz |
| $\varepsilon$ | Predefined error level | 0.001 |

acceleration-based parameters) has been shown to play an important role in daily human activity tracking and monitoring, e.g., in [11]. Here, the absolute (total) acceleration $a_n(t)$ of the moving scatterer $S_n^M$ can be obtained from the speed $v_n(t)$ as $a_n(t) = \sqrt{(dv_{n,x}(t)/dt)^2 + (dv_{n,y}(t)/dt)^2 + (dv_{n,z}(t)/dt)^2}$ ($n = 1, 2$). This quantity is depicted in Fig. 4(a) and (b) for persons $P_1$ and $P_2$, respectively. Here again, the good match between the exact and estimated accelerations stresses the validity of the estimation technique. Furthermore, we plot in Fig. 5(a) and (b) the exact TV VAOM $\alpha_n(t)$ of the persons $P_1$ and $P_2$ with the estimated angles, respectively. A good correspondence can be observed between both quantities.

It is worth mentioning that several trials have shown that a small error in the estimation of the TV direction of motion (VAOM and HAOM) does not affect the objective function $E(\mathcal{P}_p)$. It should also be emphasized that, in this section, we considered the case where the two persons $P_1$ and $P_1$ are moving with different speed models to demonstrate that the presented velocity estimation procedure remains valid regardless of the activities of the persons in the indoor area.

*Comparison with other methods:* Although it is of great importance to compare the performance of the presented velocity estimation algorithm with algorithms available in the literature, this task cannot be achieved. This is because, to our knowledge, there are no detailed studies that can be considered for this purpose. In addition, and as has been stressed in the beginning of Section I, the estimation methods developed in the context of mobile radio communication cannot be considered either because they are limited to WSS channels (the speed of the MSs is assumed to be constant) and do not provide any information regarding the direction of motion.

## V. CONCLUSION

In this paper, we propose a new RF-based iterative procedure to estimation the velocity of multiple moving objects/persons in indoor areas equipped with a distributed $3 \times 3$ MIMO system. The propagation phenomenon taking place in the indoor space is modelled by a non-stationary 3D indoor

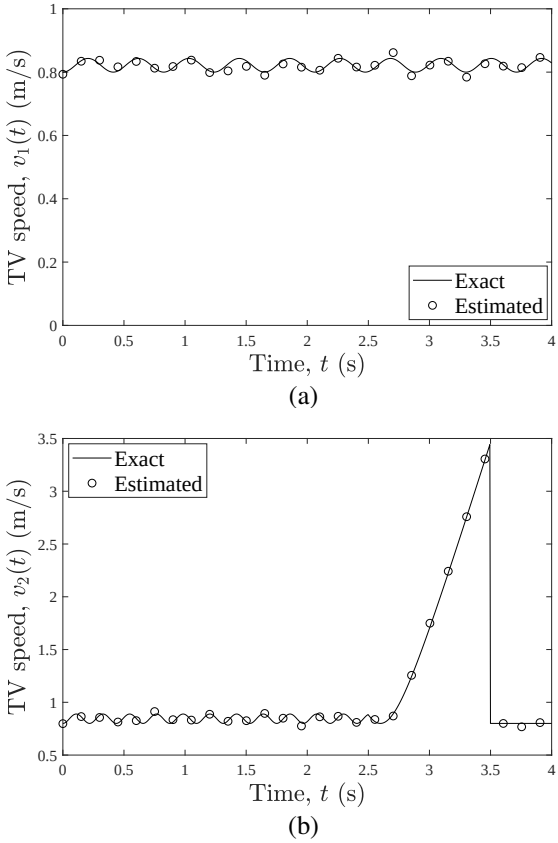


Fig. 3. TV speed (a) $v_1(t)$ of the moving scatterer $S_1^M$ (person $P_1$) and (b) $v_2(t)$ of the moving scatterer $S_2^M$ (person $P_2$).

channel model. The main aim of this method is to estimate the TV velocity, i.e., TV speed, TV VAOM, and TV HAOM, of the multiple moving persons. This task is achieved by matching the spectrogram of the channel model as close as possible to the spectrogram computed from the received RF signals. Together with the TV velocity, the proposed algorithm determines all channel parameters, e.g., path gains, phases, angles, etc. The good fit observed between the exact TV speed, TV acceleration, and TV VAOM of the different moving persons and the corresponding estimated quantities verifies the accuracy and soundness of the estimation approach.

## REFERENCES


[1] G. L. Stüber, *Principles of Mobile Communications*, Springer Int. Publishing, 4th edition, 2017.

[2] Y. Zhuang et al., "An iterative Doppler shift estimation in vehicular communication systems," *Procedia Engineering*, vol. 29, pp. 4129–4134, 2012.

[3] C. Tepedelenlioğlu, A. Abdi, G. B. Giannakis, and M. Kaveh, "Estimation of Doppler spread and signal strength in mobile communications with applications to handoff and adaptive transmission," *Wireless Commun. and Mobile Comput.*, vol. 1, no. 2, pp. 221–242, 2001.

[4] L. Krasny, H. Arslan, D. Koilpillai, and S. Chennakeshu, "Doppler spread estimation in mobile radio systems," *IEEE Commun. Letters*, vol. 5, no. 5, pp. 197–199, May 2001.

[5] H. Zhang and A. Abdi, "Nonparametric mobile speed estimation in fading channels: Performance analysis and experimental results," *IEEE Trans. Wireless Commun.*, vol. 8, no. 4, pp. 1683–1692, Apr. 2009.

[6] M. Ermes, J. Pärkkä, J. Mäntyjärvi, and I. Korhonen, "Detection of daily activities and sports with wearable sensors in controlled and uncontrolled

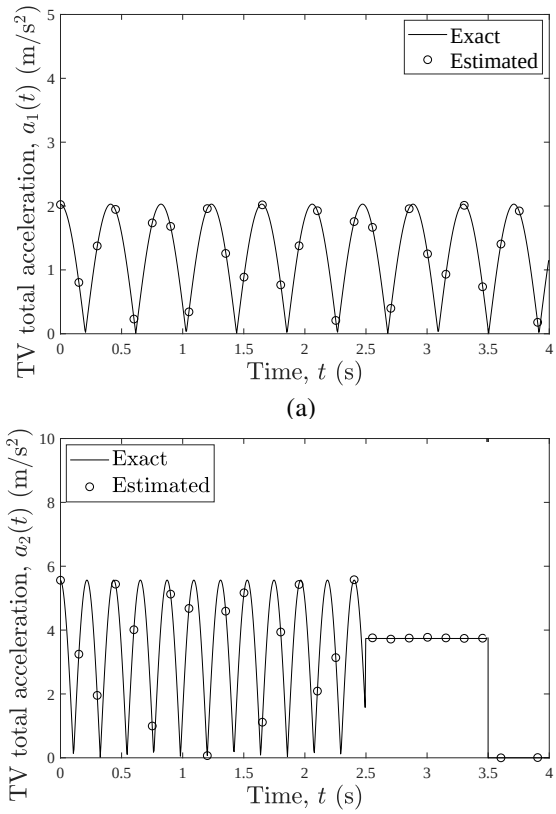


Fig. 4. TV absolute (total) acceleration (a) $a_1(t)$ of the moving scatterer $S_1^M$ (person $P_1$) and (b) $a_2(t)$ of the moving scatterer $S_2^M$ (person $P_2$).

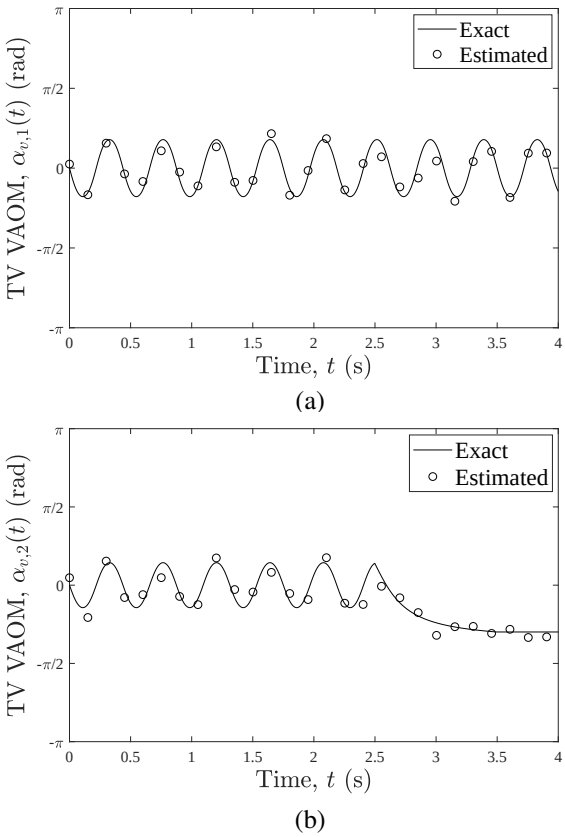


Fig. 5. TV VAOM (a) $\alpha_{v,1}(t)$ of the moving scatterer $S_1^M$ (person $P_1$) and (b) $\alpha_{v,2}(t)$ of the moving scatterer $S_2^M$ (person $P_2$).


conditions," *IEEE Trans. Inf. Technol. Biomed.*, vol. 12, no. 1, pp. 20–26, Jan. 2008.

[7] C. Strohrmann, H. Harms, C. Kappeler-Setz, and G. Tröster, "Monitoring kinematic changes with fatigue in running using body-worn sensors," *IEEE Trans. Inf. Technol. Biomed.*, vol. 16, no. 5, pp. 983–990, Sept. 2012.

[8] B. Mariani, M. C. Jiménez, F. J. G. Vingerhoets, and K. Aminian, "On-shoe wearable sensors for gait and turning assessment of patients with Parkinson's disease," *IEEE Trans. Biomed. Eng.*, vol. 60, no. 1, pp. 155–158, Jan. 2013.

[9] C. Zhang and Y. Tian, "RGB-D camera-based daily living activity recognition," *J. of Comput. Vis. Image Process.*, vol. 2, no. 4, pp. 12, 2012.

[10] H. Sakaino, "Video-based tracking, learning, and recognition method for multiple moving objects," *IEEE Trans. Circuits Sys. for Video Technol.*, vol. 23, no. 10, pp. 1661–1674, Oct. 2013.

[11] S. C. Mukhopadhyay, "Wearable sensors for human activity monitoring: A review," *IEEE Sens. J.*, vol. 15, no. 3, pp. 1321–1330, Mar. 2015.

[12] M. Meingast, T. Roosta, and S. Sastry, "Security and privacy issues with health care information technology," in *IEEE 28th Int. Conf. of the Eng. in Medicine and Biology Society (EMBS'06)*, 2006, pp. 5453–5458.

[13] Z. Yang, P. H. Pathak, Y. Zeng, X. Liran, and P. Mohapatra, "Monitoring vital signs using millimeter wave," in *17th ACM Int. Symp. on Mobile Ad Hoc Networking and Computing (ACM'16)*, 2016, pp. 211–220.

[14] C.-Y. Hsu et al., "Extracting gait velocity and stride length from surrounding radio signals," in *Proc. of the ACM Conf. on Human Factors in Computing Systems (CHI'17)*, Denver, USA, May 2017, pp. 2116–2126.

[15] Y. Wang, K. Wu, and L. M. Ni, "Wifall: Device-free fall detection by wireless networks," *IEEE Trans. Mobile Comp.*, vol. 16, no. 2, pp. 581–594, 2017.

[16] M. G. Amin, Y. D. Zhang, F. Ahmad, and K. C. D. Ho, "Radar signal processing for elderly fall detection: The future for in-home monitoring," *IEEE Signal Process. Mag.*, vol. 33, no. 2, pp. 71–80, Mar. 2016.

[17] S. Li et al., "AR-alarm: An adaptive and robust intrusion detection system leveraging CSI from commodity Wi-Fi," in *Int. Conf. on Smart Homes and Health Telematics*. Springer, 2017, pp. 211–223.

[18] R. Ramezani, Y. Xiao, and A. Naeim, "Sensing-Fi: Wi-Fi CSI and accelerometer fusion system for fall detection," in *IEEE EMBS Int. Conf. on Biomed. & Health Informat. (BHI'18)*, 2018, pp. 402–405.

[19] X. Dang et al., "PCA-Kalman: device-free indoor human behavior detection with commodity Wi-Fi," *EURASIP Journal on Wirel. Commun. and Networking*, vol. 2018, no. 1, pp. 214, 2018.

[20] Z. Jiang et al., "Communicating is crowdsourcing: Wi-Fi indoor localization with CSI-based speed estimation," *J. of Computer Science and Technol.*, vol. 29, no. 4, pp. 589–604, Jul. 2014.

[21] R. Hicheri, M. Pätzold, and N. Youssef, "Estimation of the velocity of a walking person in indoor environments from mmWave signals," in *IEEE Global Commun. Conf. (GLOBECOM'18)*, Abu Dhabi, UAE, Dec. 2018, accepted for publication.

[22] A. Abdelgawwad and M. Pätzold, "On the influence of walking people on the Doppler spectral characteristics of indoor channels," in *28th IEEE Int. Symp. on Pers., Indoor, and Mobile Radio Commun. (PIMRC'17)*, Montreal, QC, Canada, Oct. 2017.

[23] R. Hicheri, M. Pätzold, and N. Youssef, "Estimation of the velocity of a walking person in non-stationary indoor environments from the received RF signal," in *IEEE Latin-American Conf. on Commun. (LATINCOM'18)*, Guadalajara, Mexico, Nov. 2018, accepted for publication.

[24] A. Abdelgawwad and M. Pätzold, "A framework for activity monitoring and fall detection based on the characteristics of indoor channels," in *IEEE 87th Veh. Technol. Conf. (VTC'18-Spring)*, Porto, Portugal, Jun. 2018, pp. 1–7.

[25] S.-U. Jung and Mark S. Nixon, "Estimation of 3D head region using gait motion for surveillance video," in *4th Int. Conf. on Imaging for Crime Detection and Prevention (ICDP'11)*, London, UK, Nov. 2011, pp. 1–6.

[26] T. V. Barreira, D. Rowe, and M. Kang, "Parameters of walking and jogging in young adults," *Int. J. of Exercise Science*, vol. 3, no. 1, pp. 4–13, 2010.